International Journal of Thermofluid Science and Technology (2020)
Volume 7, Issue 1, Paper No. 20070102
https://doi.org/10.36963/IJTST.20070102
Research Article

Thermal Energy Storage Through Melting of a Commercial Phase Change Material in an Annulus with Radially Divergent Longitudinal Fins

Tonny Tabassum, Mainul Hasan*, Latifa Begum

Mining & Materials Engineering, McGill University, Montreal, Quebec, Canada

Received: 30 August 2019; Received in revised form: 20 December 2019; Accepted: 30 December 2019; Published online10 January 2020

Abstract

This study reports on the unsteady two-dimensional numerical investigations of melting of a paraffin wax (phase change material, PCM) which melts over a temperature range of 8.7°C. The PCM is placed inside a circular concentric horizontal-finned annulus for the storage of thermal energy. The inner tube is fitted with three radially diverging longitudinal fins strategically placed near the bottom part of the annulus to accelerate the melting process there. The developed CFD code used in Tabassum et al., 2018 is extended to incorporate the presence of fins. The numerical results show that the average Nusselt number over the inner tube surface, the total melt fraction, the total stored energy all increased at every time instant in the finned annulus compared to the annulus without fins. This is due to the fact that in the finned annulus, the fins at the lower part of the annulus promotes buoyancy-driven convection as opposed to the slow conduction melting that prevails at the bottom part of the plain annulus. Fins with two different heights have been considered. It is found that by extending the height of the fin to 50% of the annular gap about 33.05% more energy could be stored compared to the bare annulus at the melting time of 82.37 min for the identical operating conditions. The effects of fins with different heights on the temperature and streamfunction distributions are found to be different. The present study can provide some useful guidelines for achieving a better thermal energy storage system.

Keywords: longitudinal fins; natural convection melting; heat transfer; horizontal finned annulus; enthalpy-porosity technique; staggered grid

1. Introduction

In Tabassum et al., 2018, the dynamical thermal performance of the horizontal concentric circular shell and tube latent heat thermal energy storage (LHTES) unit is presented. It was found that due to the prevailing conduction mode of heat transfer at the bottom part of the annulus and for the low thermal conductivity of phase change material (PCM), the melting of PCM is very slow

**Corresponding e-mail*:Mainul.hasan@mcgill.ca

which is one of the primary bottlenecks in the applications of such LHTES units. The mushy region, which is bounded by the liquidus (59.9^0C) and solidus (51.2^0C) isotherms, was almost horizontal in shape and occupied the bottom region at the same depth after the threshold melting time of 41.18 min for all the three different inner cylinder wall temperatures. In the concentric annulus case, it was found that neither the increase in Rayleigh number nor the increase in the melting time affected the conduction dominated zone at the bottom of the annulus (about $\theta \sim 0^0$ to 80^0). How to improve the heat transfer characteristics of the PCM in a LHTES unit, particularly at the lower part is the primary motivation of this part of the study.

To resolve this inefficient heat transfer problem, the present study has specifically focused on the use of fins as a possible heat transfer enhancement mechanism for the increased storage of thermal energy at the bottom part of the annulus. It is well-known that heat transfer in a horizontal annulus is limited by the heated inner cylinder when the outer cylinder is insulated. The fins can be attached to the outer surface of the inner cylinder to increase the heat transfer area. A number of experimental and numerical studies exist in the literature concerning single-phase and multi-phase natural convection heat transfer in an annulus fitted with the various configurations of the fins.

A detail literature review concerning the melting of the phase change material with regard to the energy storage has been reported in Tabassum et al., 2018. Therefore, in this part, only the published literature concerning the melting of the PCM in various systems in the presence of internal fins are reviewed. It is to be noted that the thermal conductivity of the PCM particularly of paraffin wax and their mixtures, which have proven to be suitable for low-temperature latent heat energy storage applications, are unacceptably low. During the energy storage process (melting) the effect of the conductivity of the PCM is not very significant since the melting is predominantly controlled by natural convection in the melt. But during the energy retrieval phase, the low thermal conductivity of the PCM drastically reduces the heat transfer to the receiving medium (sink) since the solidified layer which grows on the heat transfer surface (s) offers significant thermal resistance to the conductive mode of heat transfer.

One of the methods for enhancing heat transfer in a LHTES unit is by increasing the heat transfer surface area exposed to the PCM. In this regard, the addition of fins has been suggested and studied by many investigators (Rathod and Banerjee, 2015; Kamkari and Shokouhmand, 2014; Li and Liu, 2013; Saha and Dutta, 2011; Sharifi et al., 2011; Nayak et al., 2006; Zhang and Faghri, 1996). Agyenim et al. (2009) experimentally studied the melting and solidification characteristics of a PCM (Erythritol) in a double pipe heat exchanger where the PCM was placed in three types of the annulus, namely a plain, a circular finned and longitudinal finned annuli. Their temperature measurements in the radial, circumferential and longitudinal directions revealed that in the latter two directions the gradients were below 5% of the temperature gradients in the radial direction and the authors postulated that for the heat transfer analysis, it is not necessary to take into consideration the variations in temperatures in the flow direction of the HTF. The authors further found that the longitudinal finned annulus provided the best thermal efficiency compared to the other two cases. Sciacovelli et al. (2015) reported that the heat transfer performance of shell-and-tube LHTES unit could be enhanced by tree-shaped fins. Their results showed that the solidification efficiency is increased by about 24% when fins with two bifurcations were employed. They further reported that the size and number of fins are important for phase change heat transfer characteristics. Hosseini et al. (2015) studied the melting of a PCM inside a horizontal tube with longitudinal fins. In their study, they selected fins with two different lengths and their performance was studied for three different Rayleigh numbers (Ra). The fin length was found to have a significant effect on the melting time. With the increase of fin length, the melting time was found to decrease while the depth of the melt increased. Using the commercial code ANSYS Fluent 13.0, Li and Wu in 2015 numerically studied the 3D melting and solidification problem of two phase-change materials (PCMs) in a horizontal concentric shell and tube heat exchanger. Of the two PCMs, one

was a pure $NaNO_3$ and the other was a composite of $NaNO_3$/expanded graphite. A total of six fins each having a length of 2.5 times the diameter of the inner tube was placed at equally spaced angular positions. They found that the thermal energy storage (TES) unit with extended fins resulted in a decrease of about 14% in the full melting/solidification time compared to the TES unit without fins. For the composite PCM, the full melting/solidification time was found to decrease by about 20%.

From the above literature review, it is evident that the aforementioned studies primarily focused on the effect of the shape, size, and a number of fins on the heat transfer characteristics of the PCM in a LHTES unit. All numerical studies have dealt with either pure PCM or pseudo-pure PCM. In the literature, there is no report on the quantitative analysis regarding the energy storage capabilities of the PCM in a finned-LHTES unit. Therefore, in this study, a commercial paraffin wax as a PCM in finned-annulus is considered. Also, a detailed quantitative analysis of the energy storage is reported here. In order to promote melting in the conduction dominated zone in the lower part of the annulus, three longitudinal divergent radial fins with round tips are attached to the outer surface of the inner cylinder. These fins are placed one at the symmetry plane when the installation angle of the fin (θ) is equal to 0^0, another at $\theta = 30^0$, and the third one at $\theta = -30^0$ at the bottom part of the annulus. The fin heights inside the annulus are arbitrarily set to 30% and 50% of the annulus gap ($L = r_o - r_i$). Three different fixed wall temperature (Tw) boundary conditions are selected for an initial Stefan number of zero. For the convenience of discussion, the fin height of 30% of the annulus gap (H = 0.3L) will be referred to as the short-finned annulus and the fin height of 50% of the annulus gap (H = 0.5L) will be referred to as the long-finned annulus. Through the analysis of the comprehensive heat transfer mechanism of heat conduction and natural convection heat transfer combined with the calculations of the melt fraction (f_L), the total stored energy, and the surface-averaged Nusselt number on the inner tube, all as a function of melting time are provided. A comparison between the finned-annulus and a bare annulus is also given. The results of this study can provide a reference for strategically arranged fins, based on which more efficient LHTES unit could be designed.

2. Mathematical Model

Figure 1 shows the two-dimensional physical model of a LHTES unit which has the same geometrical configuration as that depicted in Fig. 2 in Tabassum et al., 2018. In this study, three internal fins are attached to the outer surface of the inner tube at the bottom part of the annulus. The volume located between the two cylinders is filled with the PCM. The thermo-physical properties of the PCM are listed in Table 1 in Tabassum et al., 2018.

Figure 1 shows the cross-section of a horizontal annulus with three longitudinal divergent round tips fins. Two heights of a fin are selected. Each fin has a height (H) of either 16 mm (named as long fin) or 9.6 mm (named as short fin). The thickness of the above-mentioned fins is given in Table 1. The cylinder walls and the fins are assumed to be highly conducting. For the sake of presentation, in Tabassum et al., 2018 study, the LHTES unit will be called plain annulus while in the present study the LHTES unit will be called finned annulus. Since the physical domain is symmetric about the vertical centerline of the outer tube, the right-half of the annulus gap is chosen as the solution domain which is presented by the blue color in Fig. 1.

It is found that for a plain annulus presented in Tabassum et al., 2018, the cross-sectional area of the annulus gap is 72.38 cm^2, which has hold 5.718 kg of PCM when the length of the cylinder is 1.0 m. For a finned annulus though the embedding internal fin increases the heat

transfer area the volume of the fins reduces the amount of PCM in a LHTES unit. It is calculated that for a long-finned heat exchanger 5.6624 kg of PCM fills the annular gap whereas for the short-finned annulus 5.6885 kg fills the annular gap. Thus, in this study, it will be investigated how the reduction of the amount of PCM due to the presence of the embedded fins will bring benefit regarding the storage of energy by reducing the conductive thermal resistance at the bottom part of

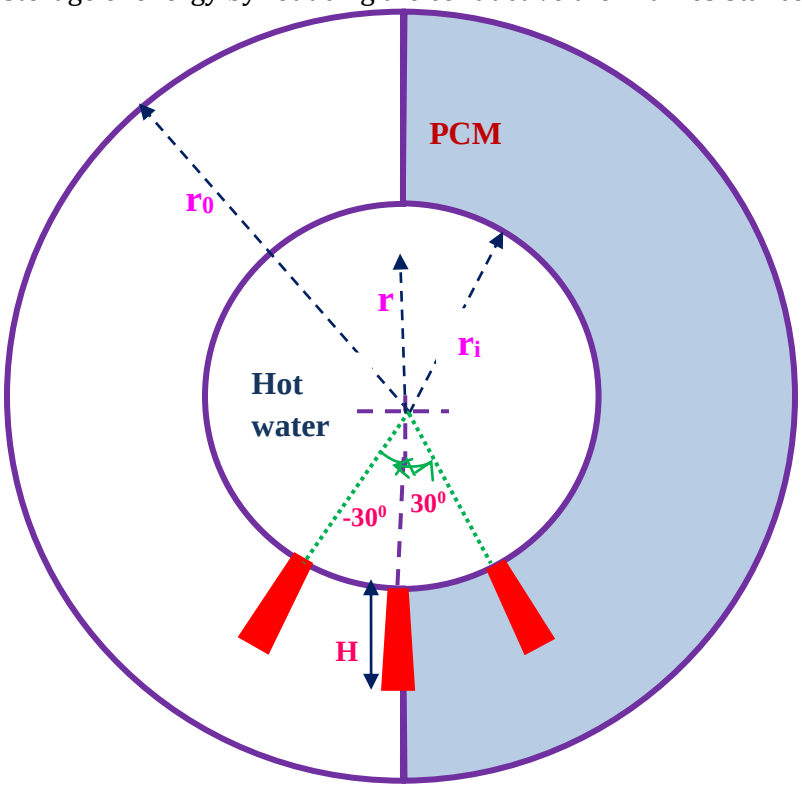

Fig. 1. Schematic view of the cross-section of the finned annulus where the blue part representing the computational domain.

Table.1. Physical properties and thickness of the solid aluminum fin.

Properties, symbol	Value [units]
Thermal conductivity (solid) (k)	0.1799 [kW / (m-K)]
Density (solid) (ρ)	2712.6 [kg/m^3]
Specific heat (solid) (C_P)	0.96 [kJ/(kg-K)]
Width of the radial divergent solid fins	
Thickness (at base)	1.0472[mm]
Thickness (at tip)-for long-fin	1.8849[mm]

Thickness (at tip)-for short-fin	1.5498 [mm]

the annulus.

2.1 Numerical formulation

The conservation two-dimensional equations in cylindrical coordinates (r-θ) in the general form can be written as follows:

$$\frac{\partial(\rho_r \varphi)}{\partial t} + \frac{1}{r}\frac{\partial}{\partial r}\left(\rho_r r u\varphi - \Gamma_\varphi r \frac{\partial \varphi}{\partial r}\right) + \frac{1}{r}\frac{\partial}{\partial \theta}\left(\rho_r v\varphi - \frac{\Gamma_\varphi}{r}\frac{\partial \varphi}{\partial \theta}\right) = S_\varphi \text{ ---------- (1)}$$

Where φ, Γ_φ, and S_φ are the general dependent variables, the generalized diffusion term, and the source term, respectively. The values of φ corresponding to mass, momentum and energy equations are 1, u, and v, and h, respectively. The associated variables Γ_φ and S_φ for all of the transport equations can be obtained by comparing the corresponding conservative equation for the variable φ.

The model assumptions, governing equations for laminar melt velocity and enthalpy in the r-θ coordinates for the phase-change problem along with the associated boundary conditions all are provided in Tabassum et al., 2018. To conserve the space these are not repeated here. An additional energy balance equation in the dimensional form for the solid fins can be writen as follows:

$$\frac{\partial(\rho_r C_P T)}{\partial t} = \frac{1}{r}\frac{\partial}{\partial r}\left(\frac{K}{C_P} r \frac{\partial(C_P T)}{\partial r}\right) + \frac{1}{r}\frac{\partial}{\partial \theta}\left(\frac{K}{C_P}\frac{1}{r}\frac{\partial(C_P T)}{\partial \theta}\right) \text{ ---------- (2)}$$

The non-dimensionalized conservative form of the energy equation for solid finis as follows:

$$\frac{\partial h^*}{\partial \tau} = \frac{\alpha_{Fin}}{\alpha_{PCM}}\frac{1}{R}\frac{\partial}{\partial R}\left(R\frac{\partial h^*}{\partial R}\right) + \frac{\alpha_{Fin}}{\alpha_{PCM}}\frac{1}{R}\frac{\partial}{\partial \theta}\left(\frac{1}{R}\frac{\partial h^*}{\partial \theta}\right) - \frac{\partial \nabla H^*}{\partial \tau} \text{ ---------- (3)}$$

To improve the melting rates, aluminum is chosen for its high thermal conductivity as the fin material for both short and long solid fins. The physical properties and dimensions of the solid aluminum fins are listed in Table 1. Detailed solution procedure, code validation, grid and time independent tests, definitions of various quantitive items, all are available in Tabassum et al., 2018 and in Tabassum (2010).

3. Results and Discussion

In order to gain a better understanding of the role of the fins during the melting process, the process parameters such as the Prandtl number, radius ratio, inner cylinder wall temperatures and the initial Stefan number were all kept the same as the plain annulus studied in Tabassum et al., 2018. In this section, the effect of the main process parameters, such as the inner tube wall temperature, the height, and the shape of the fin attached to the inner tube will be presented and discussed in detail. A comparison also will be made between the plain and fin annulus. It is to be mentioned here that in

this numerical investigation of natural convection dominated melting of an impure PCM a lot of results have been generated. It is a challenge to present those results in a concise and meaningful manner so that the readers can easily understand the studied melting phenomena influenced by the different parameters. In this regard, a total of four cases is selected which are listed in Table 2. Because of the vertical symmetry along the θ-direction, a right-half of the domain is simulated in this study.

Table 2. Computational cases studied (Pr = 40.15, diameter of the inner cylinder, D_i = 0.04 m, diameter of the outer cylinder, D_o = 0.104 m).

Case	Geometry	Initial temperature of PCM (T_i) (^oC)	Inner tube wall temperature (T_W) (^oC)	Rayleigh number (Ra)	Stefan number (Ste_w)	Melting time (t) (min)
1	Long-finned annulus	51.2	69.9	1.09×10^6	0.2116	t = 20.59, t = 41.18, t = 61.78, t = 82.37
2	Long-finned annulus	51.2	74.9	1.38×10^6	0.2682	
3	Long-finned annulus	51.2	79.9	1.67×10^6	0.3248	
4	Short-finned annulus	51.2	79.9	1.67×10^6	0.3248	

3.1 Cases (1-3) of Table 2: temperature and streamfuntion fields in the long-finned annulus.

Figures 2(a-h) display the transient progression of the isotherms and streamfuntions within the right-half of the cross-section of the long-finned annulus for four different time instants for case 1. In Figs 2(a-d), the blue color region represents the mushy zone area which is bounded by the liquidus (59.9^0C) and the solidus (51.2^0C) isotherms. Above the liquid phase interphase in the unit, all isotherms are presenting the temperatures of the melted PCM. Initially, the commercial paraffin wax melts near the inner cylinder due to conduction mode of heat transfer but as the melt layer starts to grow the convection heat transfer gradually takes over. Starting from the bottom fin placed at the symmetry axis (θ = 0^0), the melt gains heat and moves along the wall of the inner cylinder until it reaches the second fin at θ = 30^0. At this point, the melt is forced to bend and flows downward along the second fin. The melt in between the fins is trapped and is unable to follow the contour of the outer cylindrical surface. Figures 2(e-h) also show the aove fact clearly. This is mainly due to the blockage effect by the fins in the long-finned annulus. The lower surface of the second fin transfers heat only by conduction, preventing melt movement from the bay. The upper surface of the second fin enhanced the melt flow by convection adjacent to the inner cylinder wall. Because of the high thermal conductivity of aluminum, the two fins quickly attain the inner cylinder wall temperature. Due to the temperature difference, heat exchange takes place between the fins and the melt and solid PCM by conduction and convection in between the fins and around the fins. The continuous heating of the downward moving melt faces an upward force near the tip of the second fin, causing deceleration of the downward motion. As the melt approaches near the top of the inner cylinder the flow starts to bend and move downward along the outer cylinder. For a fixed inner cylinder wall temperature, with the progress of the melting time, the melt temperature inside the annulus increases, as a consequence the buoyancy force decreases. On examining the

streanfunction contours, the above-stated phenomenon can be easily seen. With the increase in the melting time the recirculation cell starts to expand sideways as well as downwards. The strength of the streamlines are decreasing at the top and increasing at the bottom part of the annulus with time.

The beneficial effect of the fins in the concentric annulus can be seen by comparing among the Figs 2(a-h) and Figs. 5(a-h) (Tabassum et al., 2018). It is evident from these figures that for finned annulus the melt volume and the mushy region increase at a much faster rate with time. The mushy

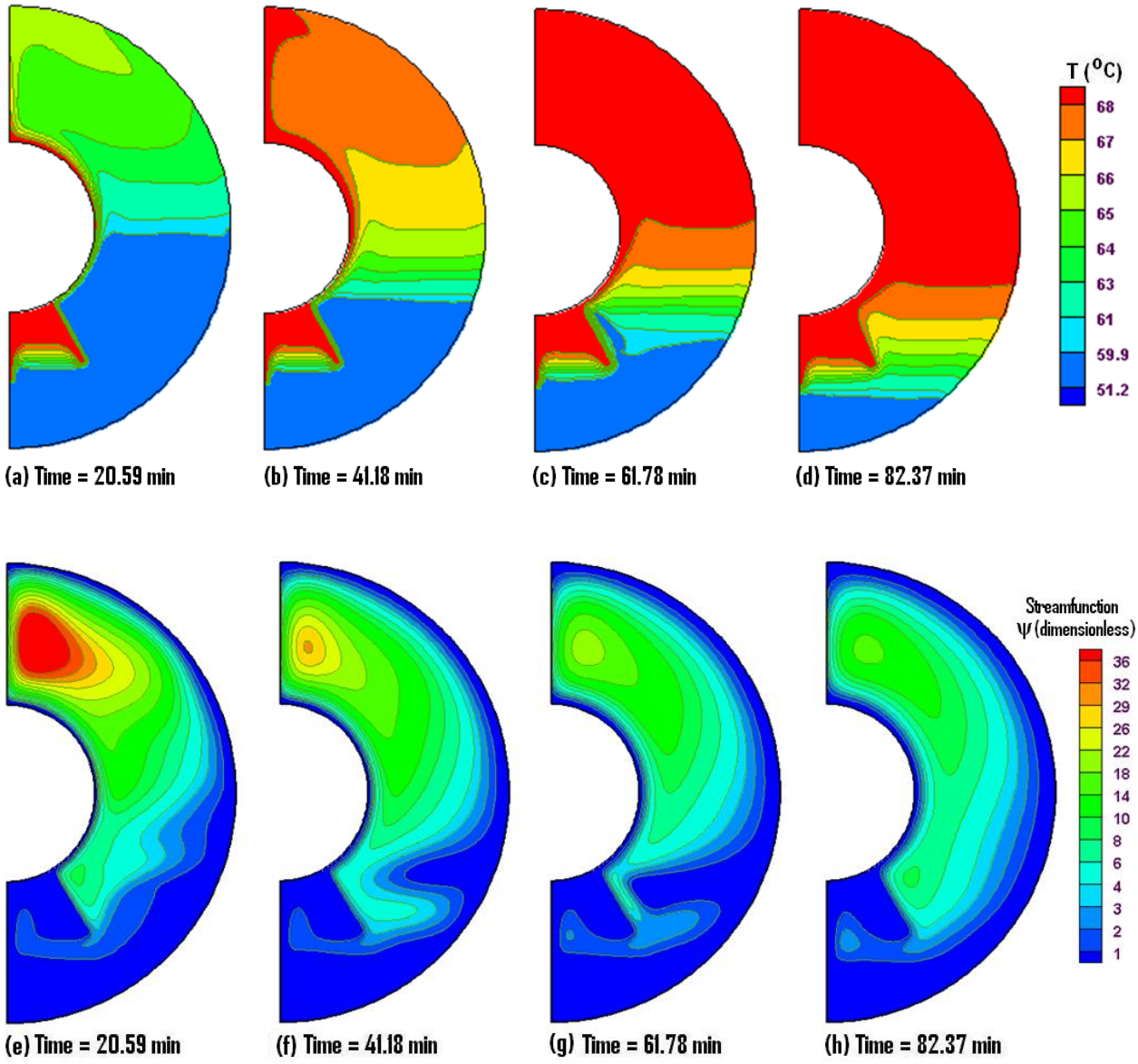

Fig. 2. 2-D views of the changes of the isotherms (a-d) and streamfunction contours (e-h) with time during the melting in a long-finned annulus for case 1.

region also gets thinner at the bottom part of the annulus compared to the plain annulus. The reason for this behavior is due to the greater convection currents in the melt at the bottom annulus

zone created by the fins. The distorted melting front around the fin tip is also observed. The progress of isotherms in between the fins can be seen to have taken parabolic shape, indicating the blockage effect created due to the fins. The local heat transfer rate is high in the blockage region. Below the middle part of the annulus, closely packed isotherms are found at a longer melting time (t = 82.37 min) which results in a high heat transfer rate in this region.

Due to the fact that Ra is relatively high in case 2 compared to case 1, the buoyancy-driven convection manifests a bit earlier and is stronger in comparison to the previous case. The movement of the mushy region represents the progression of melting inside the annulus. In Figs. 3(a-d), it is found that due to the transfer of additional heat in this case from the inner cylinder wall compared to case 1, the mushy region marches on in the gravitational direction. These local positions of the isotherms also indicate the difference between the low and high Ra. The flow field patterns are almost similar for case 1 and 2 and the blockage effect of the fins seems to have diminished after the melting time of 61.78 min for case 2, as seen in Figs. 3(e-h).

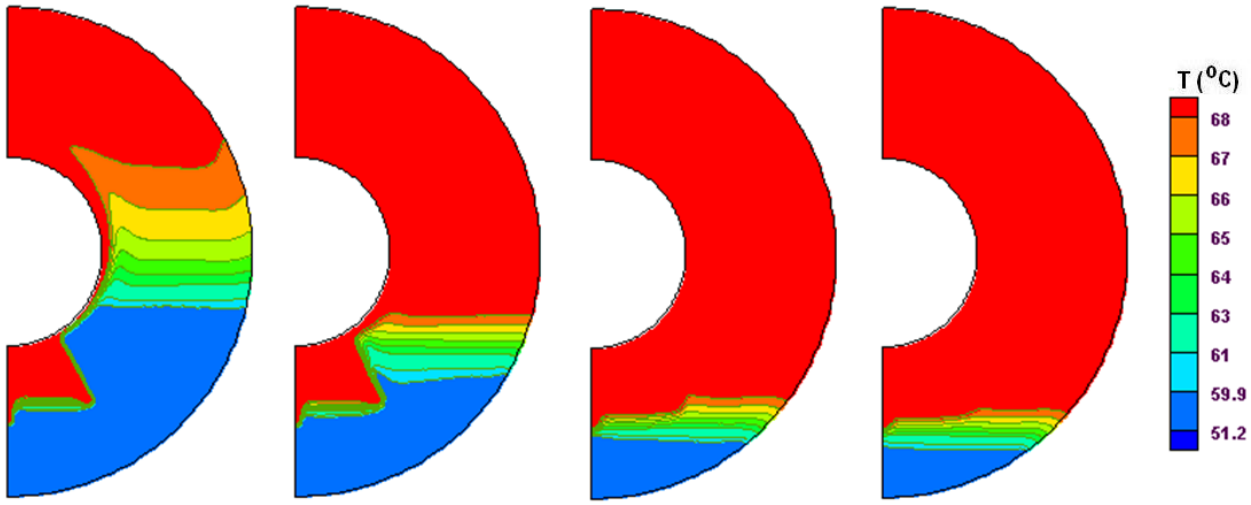

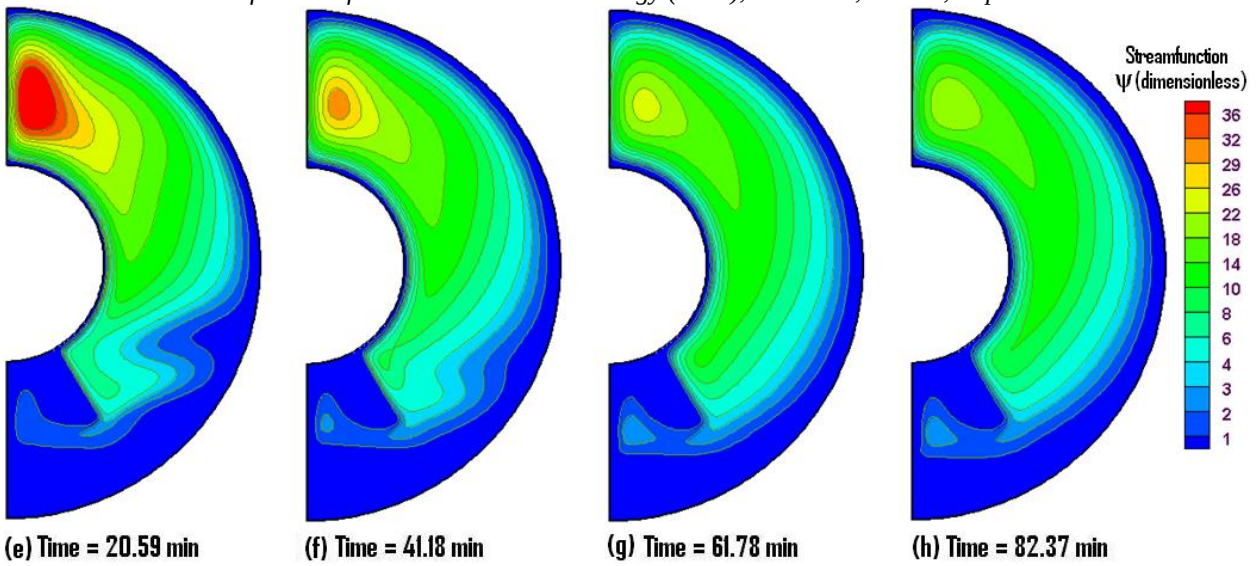

Fig. 3. 2-D views of the changes of the isotherms (a-d) and streamfunction contours (e-h) with time during melting in a long-finned annulus for case-2.

Compared to the previous two cases as Ra increases further in case 3, the convective motion of the melt is intensifying as is evidenced by the temperature and streamfunction distributions inside the annulus, depicted in Figs. 4(a-h). When Ra increases, the more closely packed isotherms found inside the annulus for a fixed time instant indicates that the local heat transfer rate is enhanced in this region. These densely packed isotherms also move toward the lower part of the annulus with the increase of melting time. The position of the mushy region is shifted more downward compared to cases 1 and 2, due to the increased convection. The blockage effect of the fin placed at $\theta = 30^0$ is prominent here up to the melting time of 20.59 min (Fig. 4(a, e)).

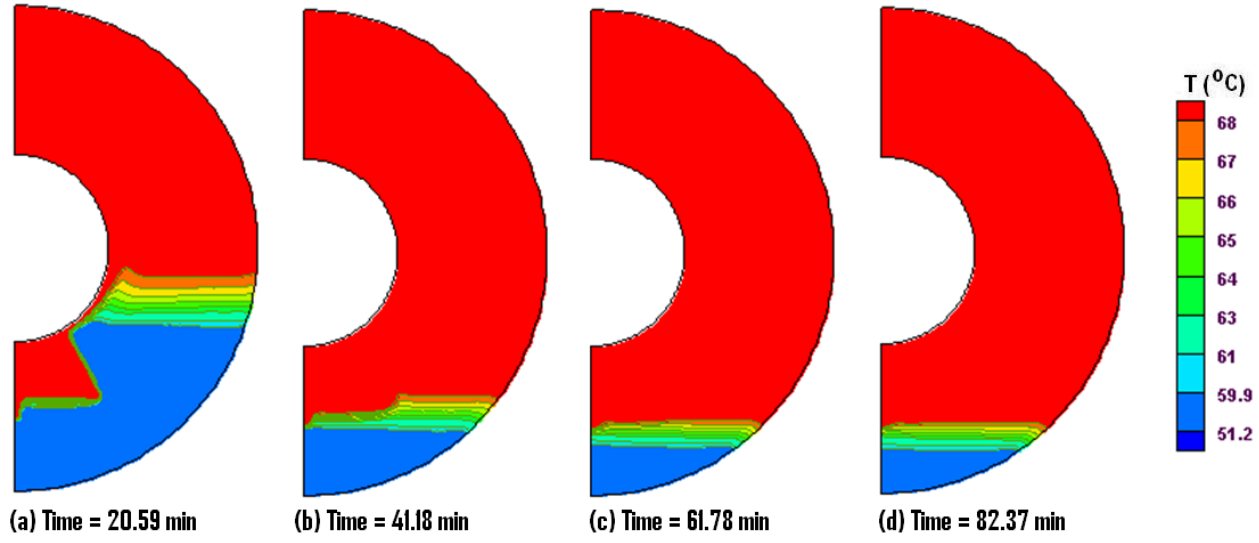

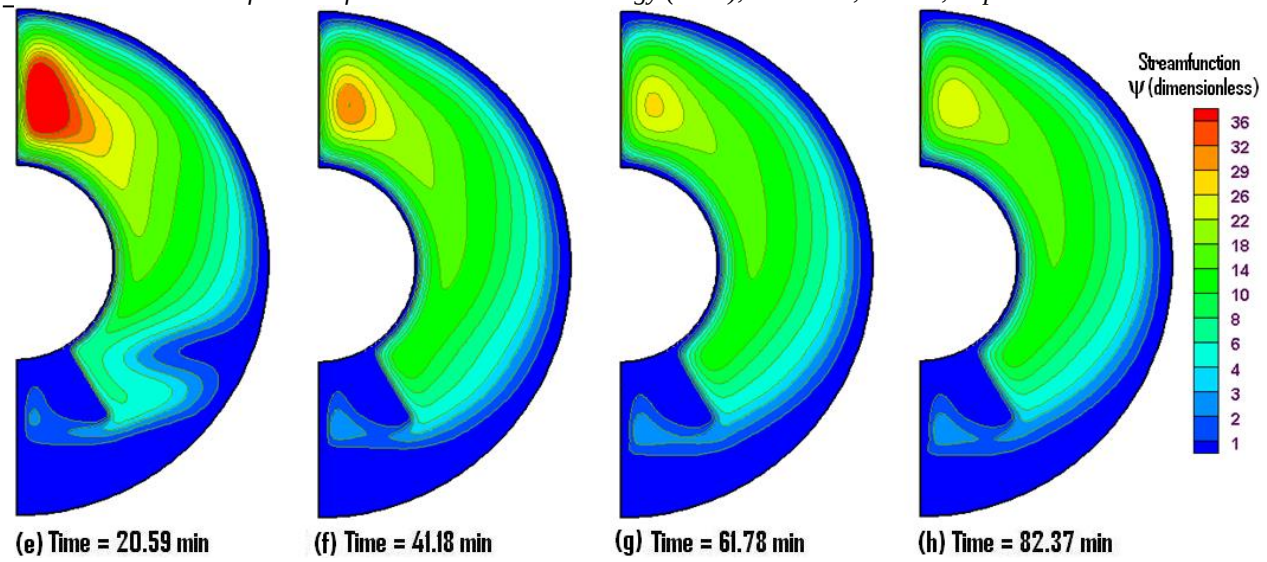

Fig. 4. 2-D views of the changes of the isotherms (a-d) and streamfunction contours (e-h) with time during melting in a long-finned annulus for case-3.

3.2. Quantitative analysis

3.2.1. Average Nusselt number ($N\bar{u}_{avg}$) for cases (1-3) of Table 2 for the long-finned annulus

The surface-averaged Nusselt number **($N\bar{u}_{avg}$)** against dimensional melting time for cases (1-3) of Table 2 for a long-finned LHTES unit are given in Fig. 5. This figure shows that the average Nusselt number decreases in three stages. The trend of the graph is similar in nature to those seen in the plain annulus case shown in Fig. 8 (Tabassum et al., 2018). The $N\bar{u}_{avg}$ is the maximum at the beginning of the melting process when the temperature difference between the inner cylinder wall and PCM is the greatest due to the conduction dominated heat transfer. With the heating going on, the melting of the PCM around the outside of the inner tube increases, as a result, the temperature of the melt approaches to that of the inner tube wall temperature and hence reduces the temperature gradient therein, consequently the $N\bar{u}_{avg}$ is decreased with a sharp negative slope, as can be seen in Fig 5, at the beginning stage of the melting process. Meanwhile, in the intermediate stage, although the natural convection effect is intensifying with time the gap between the inner cylinder wall and the solid PCM is also increasing. Thus, the beneficial effect of natural convection is reduced by the negative effect of the extended liquid layer of the PCM between the tube wall and solid PCM. The latter factor is responsible for the gradual decrease in the slope of $N\bar{u}_{avg}$ versus time curve in the second stage. With the progression of melting, all the three curves decay more gradually compared to the second stage and this is because as the melt gains heat from the inner cylinder wall it gets thermally stratified and proceeds towards the thermal equilibrium state. A threshold time of 41.18 min is found for each case in the graphs $N\bar{u}_{avg}$. After this time in all the three cases (1-3) the $N\bar{u}_{avg}$ is reduced significantly.

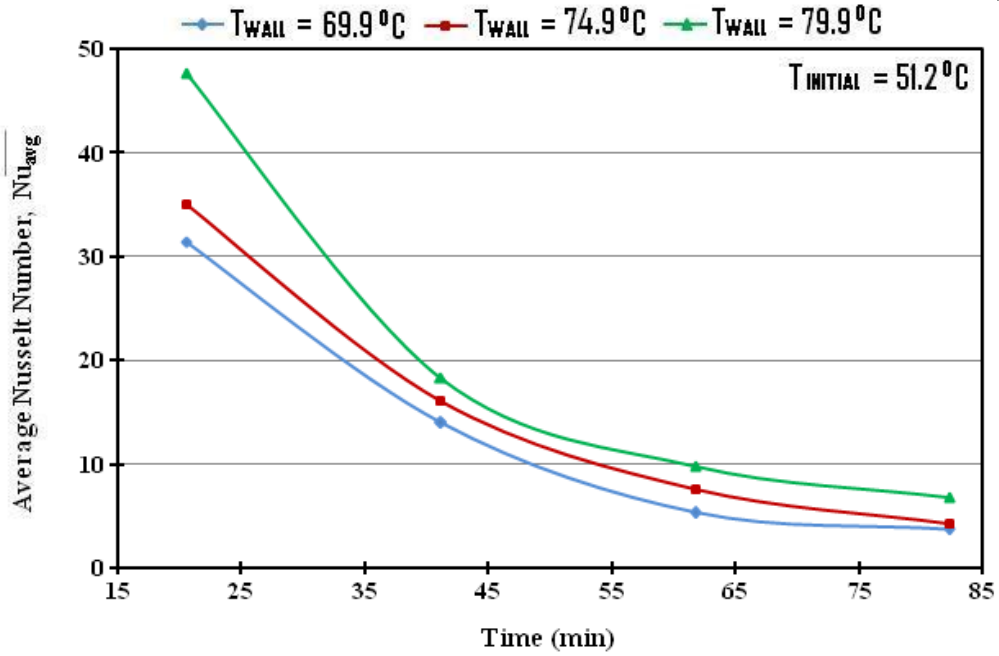

Fig. 5. Changes of the surface-averaged Nusselt numbers on the inner circular cylinder with melting time for cases (1-3) in the long-finned LHTES unit.

The increase in Rayleigh number increases the average Nusselt number as expected. The higher Rayleigh number corresponds to the higher inner tube wall temperature and thus transfers more heat from the inner tube wall to the PCM due to the increase of the thermal gradient which has resulted in strengthening the natural convection in the annulus.

The extended fins greatly increase the heat transfer area, which improves the heat transfer efficiency from the inner cylinder wall to the PCM. Thus, the LHTES unit with fin performs better than the unit without fin (Fig. 8 in Tabassum et al., 2018). The placement of the fins at the bottom part of the annulus reduces the heat resistance which occurred due to the conduction dominated heat transfer there. Therefore, for the finned annulus, a lower surface-averaged Nusselt number is obtained after a certain time instant, compared to that of the plain annulus.

3.2.2. Transient evolution of melt fraction (f_L) and the total stored energy for cases (1-3) of Table 2 for the long-finned annulus

Transient evolutions of the total liquid volume fraction and the total stored energy for cases (1-3) for the long-finned annulus are given in Figs. 6 and 7, respectively for three different Rayleigh numbers. Comparisons of the three cases indicate significant variations in each of the above quantities for a fixed time span. There is a threshold time beyond which the rate of increase of the above quantities diminishes significantly for all the three cases. This time is seen to be about 41.18 min for the studied LHTES unit and is found to be identical to the plain annulus case.

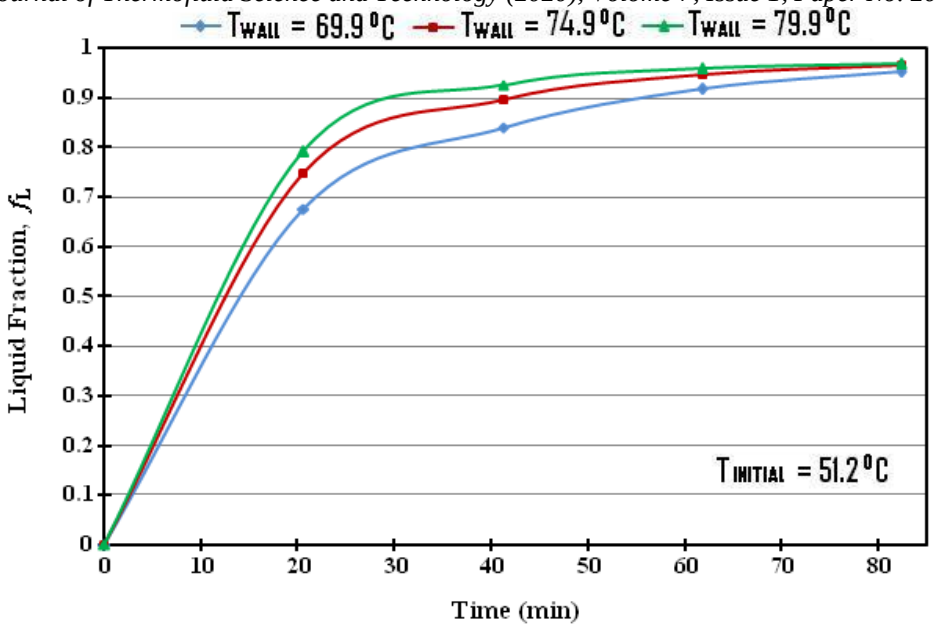

Fig. 6. Changes of the cumulative total liquid fractions with melting time for cases (1-3) in the long-finned LHTES unit.

Fig. 6 shows a very similar trend to the temporal $N\bar{u}_{avg}$ graphs (refer to Fig. 5). The rate of melting shows three stages in each of the three cases similar to the $N\bar{u}_{avg}$ graphs. The reason behind this is explained in the previous paragraph. At the time instant of 82.37 min, the melt fraction is found to be approximately 0.95, 0.96, and 0.97 in the long-finned annulus for the three cases (1-3). In case of the plain annulus, for the above time instant, the melt fraction is about 0.73, 0.74, and 0.75 for the corresponding cases (refer to Fig. 9 in Tabassum et al., 2018). For the case of the finned annulus at the melting time of 82.37 min, about 30% more PCM is melted compared to the plain annulus and the later statement is found to be true for all the three cases (1-3).

Fig. 7 shows that the amount of stored energy is enhanced considerably with the increase in melting time and for the higher values of Ra. At an elapsed time of 41.18 min, the total stored energy is 532.14 kJ/m for case 1, 590.67 kJ/m for case 2, and 639.69 kJ/m for case 3 (Fig. 7), which in comparison to the melting time of 20.59 min, is only 21.0 %, 18.63 % and 17.77 % greater, respectively. On the other hand, for case 1, after an elapsed melting time of 41.18 min, the total stored energy is only 10.24% and 5% higher for the subsequent two additional incremental time span of 20.6 min. For case 2, it is only 7.51% and 2.22% higher, whereas, for case 3, the increment is about 4.45% and 1.22%, respectively for the two subsequent time spans of each of 20.6 min. From the above analysis, it is observed that after the time instant of 41.18 min, the buoyancy-driven convection becomes weaker and weaker with time and the thermal distribution in the shell gradually tends to reach the homogeneous condition. At the end stage of melting, quite a long time is required for storing even a little amount of energy compared to the beginning and intermediate stages. Furthermore, it is observed that the rate of the incremental trend of total stored energy for a higher value of Ra is less compared to the lower value of Ra. This is because of the fact that at a higher value of Ra, the conduction mode of heat transfer takes over the convection at an earlier stage, and as a result, a less amount of sensible energy is stored.

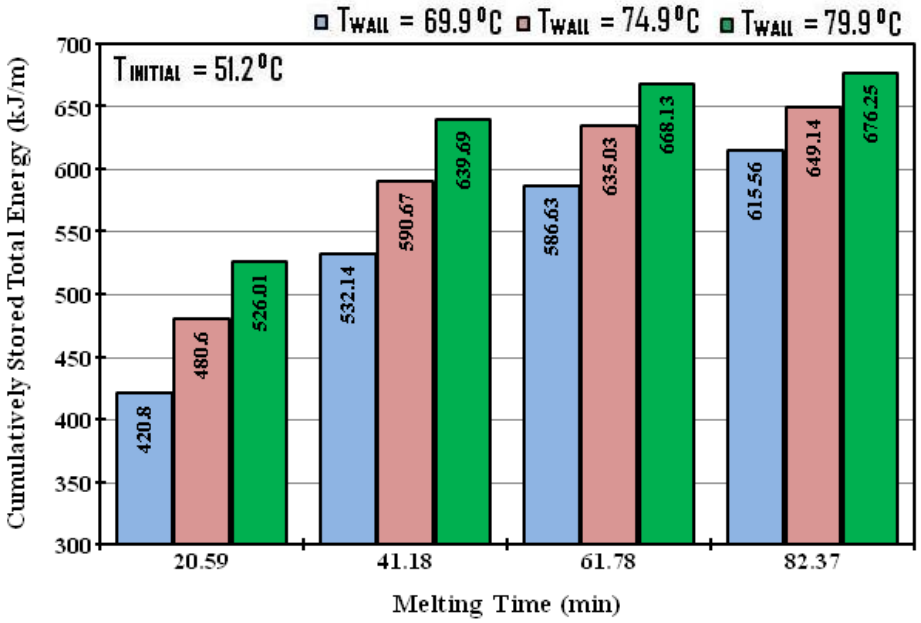

Fig. 7. Changes of the cumulatively stored total energies with melting time for cases (1-3) in the long-finned LHTES unit.

In comparison to the plain annulus (Fig. 10 in Tabassum et al., 2018), it is found that at a melting time of 82.37 min in the long-finned annulus about 32.87 % for case 1, 33.65 % for case 2, and 33.05 % for case 3 more energy is stored. The shell–tube LHTES unit with attached fins holds 2,8312 kg of PCM which is 0.0279 kg less compared to the plain annulus. Despite the less amount of PCM in a finned annulus, it stores significantly more energy due to the increased rate of the heat transfer process.

3.2.3 Comparison of the temperature and streamfnction distributions and on the total cumulative stored energy between case 3 and case 4.

To examine the influence of the height of the fin on energy storage system, two different heights of the fins are considered. In the earlier discussed case, case-3, the fin height is 50% of the annulus gap (H = 0.5L) and in case 4, the fin height is considered to be 30% of the annulus gap (H = 0.3L). Thus, due to the different heights of the fins, the shape of the annulus gap between cases 3 and 4 is altogether different.

Figures 8(a-h) representing case 4 show a similar trend in terms of the temperature fields and streamfunction contours as in case 3. Due to the change in height of the attached fin, the strength of natural convection which has a predominant effect on the energy storage during the melting process has varied and this is particularly true after the initial conduction dominated period. In general, the increase in the fin surface area, which is employed to enhance the heat transfer into the PCM, has increased the melting rate. The convection flow is also accelerated by the increase of fin height which can clearly be seen from the temperature fields prevailing in Fig. 4(a-d). All of the temperature distribution figures show that this accelerated heat pushes the mushy region more

downward than does the short-finned annulus. An inspection of the temperature isotherms and streamfunction contours clearly indicates the effect of blockage in between the short fins. In case 3, the blocage effect is diminished earlier than case 4 because of the additional heat supplied by the fin due to its 20% more fin height.

From Figs. 8(d) and 4(d), it can be seen that at the melting time of 82.37 min, the total melted fraction for the short-finned, and for the long-finned annulus is 0.93, and 0.97, respectively. The enhanced strength of the natural convection inside the long-finned annulus which in turns has led to a higher rate of melting. A comparison of the total stored energy between the two cases is shown in Table 3. It is seen that more energy is stored for case 3 compared to case 4 at every instant of time. At the final simulated melting time of 82.37 min, about 4.36 % more energy is stored in the long-finned annulus (case 3) compared to the short-finned annulus (case 4). In short-finned annulus, the total energy storage is enhanced remarkably up to the melting time of 41.18 min and after this time period, the thermal energy storage slows down similar to the long-finned annulus.

In comparison to the plain annulus, in the short-finned annulus, the total stored energy is about 21.6 % higher at the melting time of 82.37 min for the Rayleigh number of $Ra = 1.67 \times 10^6$ and for $Ste_i = 0$, suggesting that a stronger overall convection effects are at play during the melting process for the short-finned annulus.

Therefore, in terms of energy storage, the long-finned annulus is always preferable for the melting process than the short-finned annulus.

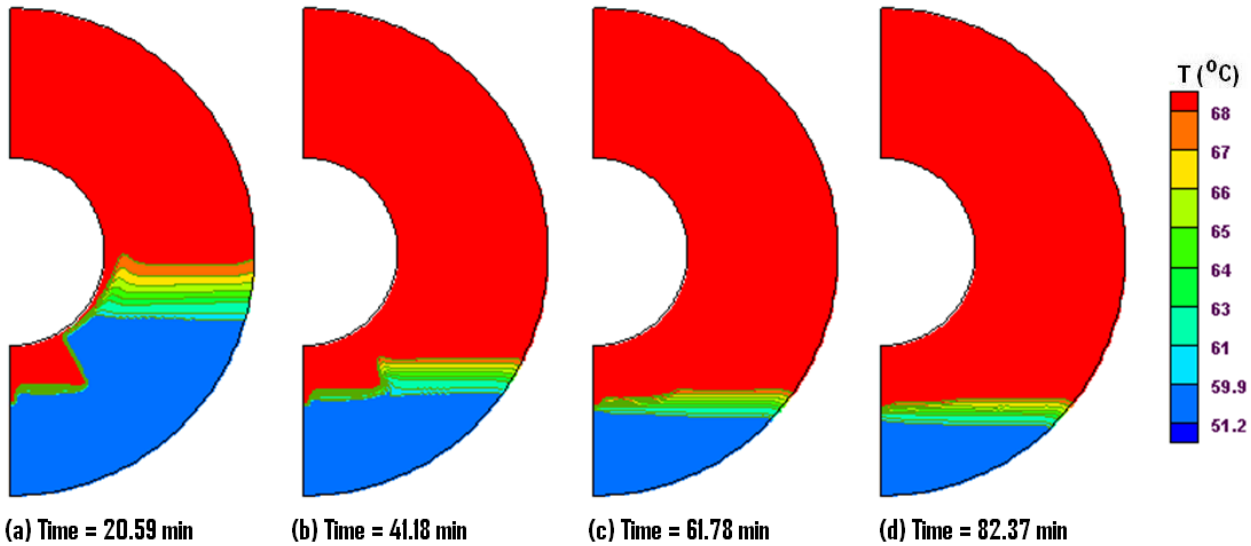

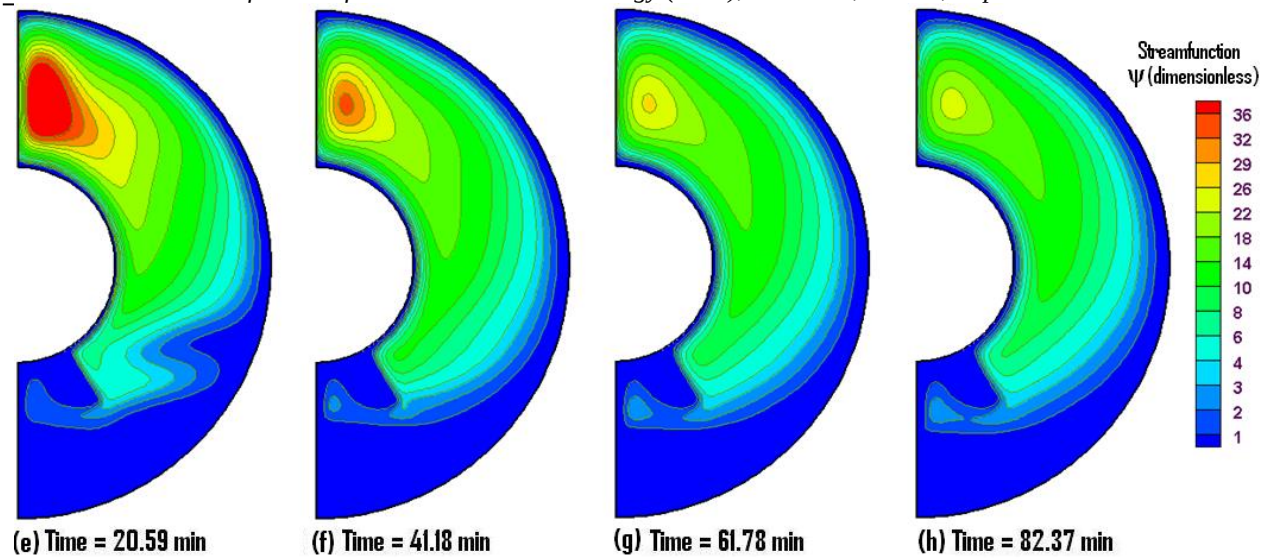

Fig. 8. 2-D views of the changes of the isotherms (a-d) and streamfunction contours (e-h) with time during the melting in a short-finned annulus for case 4.

Table 3 The cumulatively stored total energy (kJ/m) for case 3 (long-finned annulus) and for case 4 (short-finned annulus) for four different time instants.

Geometry	Melting time (min)			
	20.59	41.18	61.78	82.37
Total stored energy in long-finned annulus(kJ/m)	526.01	639.69	668.13	676.25
Total stored energy in short-finned annulus(kJ/m)	491.01	595.19	630.51	648.02

4. Concluding Remarks

In this work, the effect of the geometrical configuration of the LHTES unit with and without extended fins is systematically studied. From the present comprehensive 2-D CFD modeling study the following conclusions can be drawn:

[1]. The amount of melt is increased as the melting process continues for all the studied LHTES devices i.e., for all the cases.

[2]. At the early stage of melting, the conduction heat transfer dominates the melting process for all cases. Then with the progression of melting, in the top region of the annulus, a pear-shaped thermal plume is observed due to the initiation of the natural convection in the melt.

[3]. As the melt flows along the inner tube it gains heat, as a result, the density of the liquid PCM decreases compared to the solid PCM which manifests in the increased strength of the

buoyancy-driven convection in the top region, and thereby the melting in the top part of the annulus is much fastest than in the other regions at each elapsed time.

[4]. For a fixed time instant and for a fixed initial temperature of the solid PCM, an increase in the Rayleigh number increases the melting of PCM due to the increase in the intensity of natural convection, particularly at the top part of the annulus.

[5]. For a fixed initial temperature of the solid PCM, the surface-averaged Nusselt number decreases with the increase in the melting time in three stages. At the first stage of melting the reduction rate is remarkably high compared to the intermediate and last stages due to the intensified natural convection therein. In the latter two stages, the rate of the decease of the average Nusselt number slows down due to the gradual attainment of the thermal stratification. With the increase in the Rayleigh number, the averaged Nusselt number increases.

[6]. The high thermal conductivity of aluminum fins at the lower part of the annulus play an important role in the melting process by generating strong convective and conductive modes of heat transfer. The finned cylinder, with identical boundary conditions as the plain annulus, does promote more heat transfer and bring about totally different melting patterns. The presence of fins increased the energy storage of the heat exchanger by increasing the melting rate of the PCM compared to the plain geometry.

[7]. When the fin height is taken into consideration, it is observed that the longer fins show a better thermal performance than the shorter fins.

From this study, it is revealed that for a horizontal double pipe storage system a good way to enhance the latent heat thermal storage capacity is by placing long fins with high thermal conductivity at the lower part of the annulus.

Nomenclature

$\bar{Nu}_{avg}$ circumferential average Nusselt number based on cylinder radius

P pressure, Pa

Pr Prandtl number = $\frac{\nu_f}{\alpha_f}$

r_i radius of inner cylinder [m]

r_o radius of outer cylinder [m]

R_i dimensionless radius of inner cylinder

R_o dimensionless radius of outer cylinder

Ra Rayleigh number = $\frac{g\beta_{PCM}\left(T_{WALL}-T_{SOLIDUS}\right)D_i^3\rho}{\mu_{PCM}\alpha_{PCM}}$

Ra* modified Rayleigh number = $\frac{Ra}{Ste}$

Ste Stefan number $= \frac{C_P\left(T_{WALL}-T_{SOLIDUS}\right)}{\lambda}$

T temperature [^{0}C]

T_{WALL} inner cylinder wall temperature [^{0}C]

T_i initial temperature of the working materials [^{0}C]

t time

h^* dimensionless enthalpy $= \frac{C_P\left(T-T_{SOLIDUS}\right)}{\lambda}$

h^*_{WALL} dimensionless enthalpy at the inner wall

h^*_i initial dimensionless enthalpy in the domain

θ , r Polar coordinates, degree and m

Greek symbols

α thermal diffusivity [m^{2}s^{-1}]

β_f coefficient of thermal expansion, $-\left(\frac{1}{\rho}\right)\left(\frac{\partial\rho}{\partial T}\right)_P$, K^{-1}

ν_f kinematic viscosity [m^{2}s^{-1}]

ρ density [kg.m^{-3}]

μ dynamic viscosity [kg.m^{-1}.s^{-1}]

λ latent heat of fusion [kJ.kg^{-1}]

ΔH nodal latent heat

τ Fourier number, $\frac{t\alpha_{PCM}}{D_i^2}$

f_l	fluid fraction

Subscripts

L	liquid
S	solid
i	inner cylinder
o	outer cylinder

Superscripts

*	non-dimensional variable

Acknowledgments

This work is partially supported by the National Sciences and Engineering Research Council (NSERC) of Canada Discovery Grant RGPIN48158 awarded to M. Hasan of McGill University, Montreal, for which authors are grateful.

Funding Source

None

Conflict of Interest

None

References

Agyenim, F., Eames, P., Smyth, M., 2009. A comparison of heat transfer enhancement in a medium temperature thermal energy storage heat exchanger using fins, Sol. Energy, 83(9), 1509–1520.

Hosseini, M.J., Ranjbar, A.A., Rahimi, M., Bahrampoury, R., 2015. Experimental and numerical evaluation of longitudinally finned latent heat thermal storage systems, Energy Buildings 99, 263–272.

Kamkari, B., Shokouhmand, H., 2014. Experimental investigation of phase change material melting in rectangular enclosures with horizontal partial fins, Int. J. Heat Mass Transfer 78(11), 839–851.

Li Z., Wu, Z., 2015. Analysis of HTFs, PCMs and fins effects on the thermal performance of shell–tube thermal energy storage units, Solar Energy 122, 382–395.

Li, Y., Liu S., 2013. Effects of different thermal conductivity enhancers on the thermal performance of two organic phase-change materials: paraffin wax RT42 and RT25, J. Enhanced Heat Trans. 20(6), 463-473.

Nayak, K.C., Saha, S.K., Srinivasan, K., Dutta, P., 2006. A numerical model for heat sinks with phase change materials and thermal conductivity enhancers, Int. J. Heat Mass Transfer 49(11), 1833–1844.

Rathod, M.K., Banerjee, J., 2015. Thermal performance enhancement of shell and tube latent heat storage unit using longitudinal fins, Appl. Therm. Eng., 75(6), 1084–1092.

Saha, S.K., Dutta, P., 2011. Effect of Melt Convection on the Optimum Thermal Design of Heat Sinks with Phase Change Material, J. Enhanced Heat Trans. 18(3), 249-259.

Sciacovelli, A., Gagliardi, F., Verda, V., 2015. Maximization of performanceof a PCM latent heat storage system with innovative fins, Appl. Energy 137, 707–715.

Sharifi, N., Bergman, T.L., Faghri, A., 2011. Enhancement of PCM melting in enclosures with horizontally-finned internal surfaces, Int. J. Heat Mass Transfer 54(19), 4182–4192.

Tabassum, T., Hasan, M., Begum, L., 2018. Thermal Energy Storage Through melting of a commercial phase change material in a horizontal cylindrical annulus, Journal of Enhanced Heat Transfer DOI:10.1615/JEnhHeatTransf.2018024676, 25(3), 211-237.

Tabassum, T., 2010. A numerical study of a double pipe latent heat thermal energy storage system, M.Eng. thesis, Dept. of Mining and Materials Engineering, McGill University, Montreal, Quebec, Canada.

Zhang, Y.W., Faghri, A., 1996. Heat transfer enhancement in latent heat thermal energy storage system using an external radial finned, J. Enhanced Heat Trans. 3(2), 119-127.